Journal of Materials Chemistry A

ROYAL SOCIETY OF CHEMISTRY

PAPER

View Article Online
View Journal | View Issue

Cite this: J. Mater. Chem. A, 2021, 9, 19770

Improving quantum efficiency in organic solar cells with a small energetic driving force†

Haiqin Liu, Mengyang Li, Hongbo Wu, Jie Wang, Zaifei Ma * and Zheng Tang *

Received 21st January 2021
Accepted 23rd March 2021

DOI: 10.1039/d1ta00576f

rsc.li/materials-a

Organic solar cells based on a polymer donor (**PM7**) and a non-fullerene acceptor (**Y5**) with a very small energetic difference between the local excited state and the charge transfer (CT) state are investigated. We find that the small energetic difference (ΔE_{CT}) leads to a low voltage loss (0.44 eV). However, the short-circuit current density (J_{sc}) of the solar cell based on **PM7**:**Y5** is very low, due to monomolecular recombination of the CT state excitons, limiting the internal quantum efficiency of the device. To solve the problem with the inefficient exciton dissociation, a polymer donor (**PBDB-T**) with a similar chemical structure to **PM7** is employed as a second donor component for constructing ternary solar cells. We find that the frontier energy levels of the two donors are hybridized, allowing us to realize fine-tuning of the effective energy of the CT state and ΔE_{CT} of the ternary blend, by varying the **PBDB-T** content. As a result, a significantly improved CT state dissociation efficiency is achieved by adding a small amount of **PBDB-T** in the active layer. Meanwhile, the low voltage loss property of **PM7**:**Y5** is very well maintained in the ternary solar cell, due to the energy level hybridization of the donor materials.

1. Introduction

The development of non-fullerene acceptor materials in the last few years has increased the power conversion efficiency (PCE) of the bulk-heterojunction (BHJ) organic solar cells up to 17–18%.[1–4] Many of the highly efficient solar cells are realized based on the ternary concept consisting of adding an additional donor or acceptor into the binary BHJ active materials system:[5–7] The use of the third component can often lead to improved spectral coverage for photon harvesting and a more desired phase separation in the active layer for a more efficient charge carrier collection. Today, high quantum efficiencies (QE) are observed in organic solar cells based on different donor–acceptor combinations, and the short-circuit current density (J_{sc}) of the most efficient organic solar cells has already exceeded 25 mA cm^{-2}.[8–10] Thus, it has become increasingly more important to increase the open-circuit voltage (V_{oc}) to further improve the performance of organic solar cells.

Minimizing the voltage lost in the indispensable charge transfer process in organic solar cells is crucial. Generally, voltage losses (V_{loss}) in organic solar cells can be divided into three parts.[11–18] ΔE_{CT}, ΔV_r, and ΔV_{nr}. ΔE_{CT} (also known as the energetic driving force) is defined as the energetic difference between the charge transfer (CT) state and the local excited state of the donor or the acceptor material (S_1). The typical value for ΔE_{CT} is in the range of 0.05 to 0.2 eV for the most efficient organic solar cells. ΔV_r and ΔV_{nr} are the voltage loss terms related to the radiative and non-radiative decay rate of CT states, respectively.[15,19,20] Because the CT state can be regarded as the lowest energy of state in the blend photoactive layer,[21,22] increasing the energy of CT state (E_{CT}) for a reduced ΔE_{CT} can directly lead to a reduced V_{loss} in the solar cell. Besides, the higher E_{CT} can result in a reduced ΔV_{nr}, due to the weakened electronic coupling between the vibrational excited and ground states.[17] Furthermore, the coupling between S1 and CT state is stronger in the blend system with a higher E_{CT} and a smaller ΔE_{CT}. This can lead to a further weakened CT to ground state coupling.[16,19] As a result, the non-radiative decay rate of CT states in the blend system with a smaller ΔE_{CT} is slower, and ΔV_{nr} of the solar cell with a smaller ΔE_{CT} is lower.

However, the strong coupling between S1 and CT states in the blend active layer with a too-small ΔE_{CT} can lead to inefficient exciton dissociation, which limits QE and thus J_{sc} of the solar cell. This has been observed in solar cells based on several different BHJ systems.[23–26] The inefficient exciton dissociation can be ascribed to a rapid back transfer of CT states to S1 states, enabled by the small ΔE_{CT} at the heterointerfaces.[27] This reduces the probability for the CT state to dissociate into free charge carriers, since the energy of the free charge carrier state (E_{FC}) is generally higher than that of the CT state.[28] Therefore, there is always a tradeoff between QE and V_{loss} which must be balanced to construct efficient organic solar cells using the blends with small ΔE_{CT}. Currently, there is no solution for the poorly performing solar cells with QE limited by a too-small

State Key Laboratory for Modification of Chemical Fibers and Polymer Materials, Center for Advanced Low-dimension Materials, College of Materials Science and Engineering, Donghua University, Shanghai, 201620, P. R. China. E-mail: ztang@dhu.edu.cn; mazaifei@dhu.edu.cn

† Electronic supplementary information (ESI) available. See DOI: 10.1039/d1ta00576f

ΔE_{CT}, apart from designing new materials with different frontier energy levels.

In this work, a ternary blend strategy is employed to solve the high QE loss problem in the low V_{loss} organic solar cells based on low ΔE_{CT} systems. First, we perform a detailed investigation on the organic blend system based on poly[4,8-bis[5-(2-ethylhexyl)-4-chloro-2-thienyl]benzo[1,2-*b*:4,5-*b*′]dithiophene-2,6-diyl]-2,5-thiophenediyl[5,7-bis(2-ethylhexyl)-4,8-dioxo-4*H*,8*H*-benzo[1,2-*c*:4,5-*c*′] dithiophene-1,3-diyl]-2,5-thiophenediyl] (**PM7**) and (2,2′-((2*Z*,2′*Z*)-((12,13-bis(2-ethylhexyl)-3,9-diundecyl-12,13-dihydro[1,2,5]thiadiazolo[3,4e]thieno[2″,3″:4′,5′]thieno[2′,3′:4,5] pyrrolo[3,2-*g*]thieno [2′,3′:4,5] thieno[3,2-*b*]indole-2,10-diyl)bis(methanylylidene))bis (3-oxo-2,3-dihydro-1*H*-indene-2,1-diylidene))dimalononitrile) (**Y5**) with a very small ΔE_{CT} (close to 0 eV), and we identify a very low V_{loss} (0.44 V) in the solar cell associated with the small ΔE_{CT}. However, the ΔE_{CT} is too-small, providing an insufficient driving force for CT states to dissociate. This limits QE and J_{sc} of the solar cell. To overcome this problem, poly[(2,6-(4,8-bis(5-(2-ethylhexyl)thiophen-2-yl)-benzo[1,2-b:4,5-b′]dithiophene))-alt-(5,5-(1′,3′-di-2-thienyl-5′,7′-bis(2-ethylhexyl)benzo [1′,2′-c:4′,5′-c′]dithiophene-4,8-dione) (**PBDB-T**) with a chemical structure similar to **PM7** is introduced as a third component for constructing ternary solar cells. We find that the addition of **PBDB-T** can lead to a hybridization of the frontier orbitals of the donor materials. As a result, fine-tuning of the effective E_{CT} and ΔE_{CT} of the ternary solar cell is achieved by varying the **PBDB-T** content: a significantly improved CT state dissociation efficiency, and thus an increased QE is realized by adding a small amount of **PBDB-T** ((**PBDB-T** : **PM7** donor ratio = 10 wt%)) in the photoactive layer. More importantly, we find that the low V_{loss} property of the **PM7**:**Y5** blend is well kept in the ternary solar cell with a low **PBDB-T** content, due to the hybridization of the energy levels of the donor materials.

2. Results and discussion

Fig. 1a shows the chemical structures of the active materials used in this work. First, we focus on investigating the V_{oc} (0.98 V, Table 1) of the solar cell based on **PM7** : **Y5** (ref. 29 and 30) (1 : 1.2, weight ratio), which is higher than any of the other solar cells based on **PM7** and the Y-series acceptors reported in literature.[31,32] To understand the reason for the high V_{oc}, optical transitions in the BHJ system is investigated. The absorption properties of the blend and the pure acceptor material are studied using sensitive external quantum efficiency (EQE) and electroluminescence (EL) measurements, as shown in Fig. 1b. From the onset of the EQE spectrum, we determine E_{CT}, using a Gaussian fit derived based on the Marcus theory:[12,33,34]

$$\mathrm{EQE}(E) = \frac{fE}{\sqrt{4\pi\lambda kT}} \exp\left(-\frac{(E_{CT}+\lambda+E)^2}{4\lambda kT}\right) \quad (1)$$

where E is photon energy, k is the Boltzmann constant, T is temperature, λ is the reorganization energy, and f is a pre-factor, proportional to the density of the ground states formed at the donor–acceptor interfaces and the absorption oscillator strength of CT state (f_{osc}).

More specifically, to avoid an arbitrary fitting on the EQE spectrum, a series of fittings are performed: radiative recombination limit of the voltage loss derived using the detailed balance theory[35] is employed for determining the minimum value for E_{CT}, while the upper limit for E_{CT} is restricted by the assumption that the contribution of the weak CT state absorption to the EQE of the solar cell is at most 10%.[12,36] These boundary conditions allow us to identify a range for the values of E_{CT} with real physical meaning, and the upper and the lower boundary values are found to differ by only about 0.02–0.04 eV. For the analysis of the energetics and voltage losses in the solar cells studied in this work, the mean value of the range is used. More details regarding the fitting of the EQE spectrum are provided in ESI (SI-2).†

The value of E_{CT} from the EQE spectrum for the solar cell based on **PM7**:**Y5** is found to be very close to the energy of the optical bandgap (E_g) of the active layer, which is equivalent to the energy of the singlet excited state of the acceptor material ($E_{S1,A}$) (ESI-3†).[37] Therefore, ΔE_{CT} is very small, approaching zero.

Furthermore, the radiative recombination limit for the saturation current ($J_{0,rad}$) is also calculated from the EQE spectrum using the detailed balance theory:[11,38]

$$J_{0,rad} = q\int \mathrm{EQE}(E)\phi_{BB}(E)\mathrm{d}E \quad (2)$$

where q is the elementary charge and ϕ_{BB} is the black body spectrum at 300 K. The calculated values are listed in Table 1. From $J_{0,rad}$, we further calculate $V_{oc,rad}$, the maximum V_{oc} of the solar cell in which only radiative recombination exists.

$$V_{oc,rad} = \frac{kT}{q}\ln\left(\frac{J_{sc}}{J_{0,rad}}\right) \quad (3)$$

We find that $V_{oc,rad}$ of the solar cell based on **PM7**:**Y5** is 1.10 V, thus ΔV_{nr} is very low, only 0.12 V ($\Delta V_{nr} = V_{oc,rad} - V_{oc}$). Therefore, recombination of charge carriers in the solar cell is expected to be highly emissive. The low ΔV_{nr} of the solar cell and the high emission efficiency of CT state recombination are also confirmed by directly measuring the external quantum efficiency of electroluminescence ($\mathrm{EQE_{EL}}$) of the solar cell, which is close to 1%, corresponding to a ΔV_{nr} value of 0.13 V $\left(\Delta V_{nr} = \frac{kT}{q}\ln\left(\frac{1}{\mathrm{EQE_{EL}}}\right)\right)$.[12,38] The value of ΔV_{nr} from $\mathrm{EQE_{EL}}$ agrees very well with that calculated from $V_{oc,rad}$. Consequently, due to the small ΔE_{CT} and low ΔV_{nr}, the total voltage loss defined as $\frac{E_{S1,A}}{q} - V_{oc}$ is also very low for the solar cell based on **PM7**:**Y5** (0.44 V), considerably lower than the generally reported V_{loss} for organic solar cells (0.5–0.6 V).[39,40]

J_{sc} of the solar cell based on **PM7**:**Y5** is rather low, because IQE of the solar cell calculated using a transfer matrix model is only about 30% (ESI-4†).[41,42] For organic solar cells, a low IQE is normally due to the bimolecular recombination loss of charge carriers.[43–46] However, fast bimolecular recombination in the solar cell often leads to a low $\mathrm{EQE_{EL}}$ and a high ΔV_{nr}, contradictory to the experimental results discussed above. Therefore, light intensity dependent current density–voltage (J–V) (Fig. 1c) measurements are performed on the solar cell based on

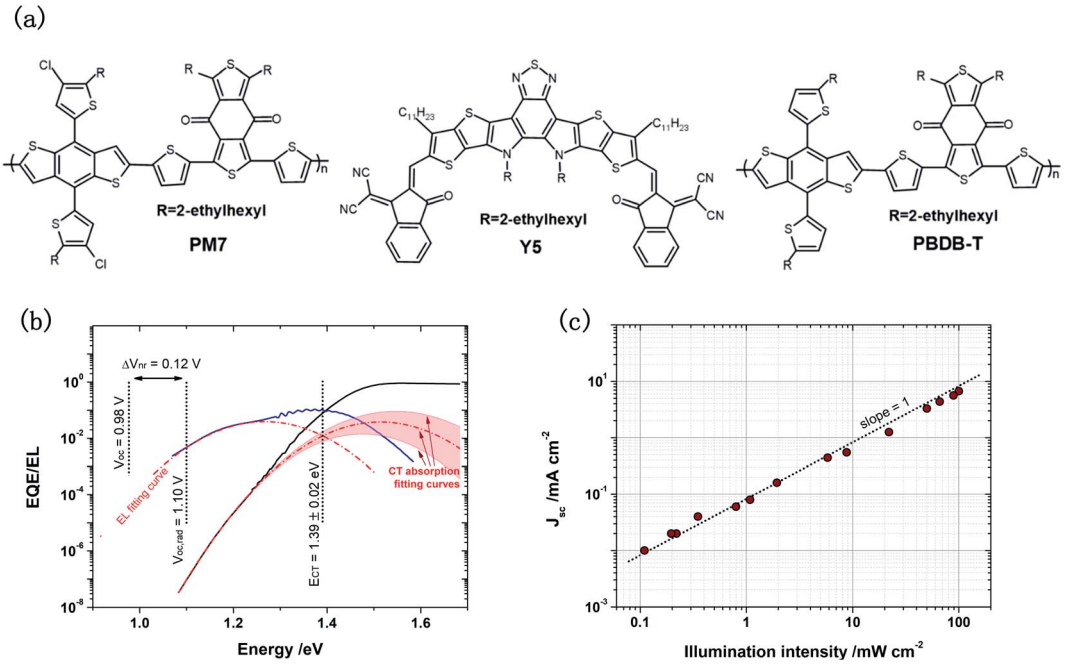

Fig. 1 (a) Chemical structures of the active materials used in this work. (b) EQE and EL of the solar cell based on PM7 : Y5 (1 : 1.2 wt ratio). The tail of the EQE spectrum is calculated from the measured EL using the reciprocal relation, and it is used to calculated E_{CT} based on the Marcus theory. $V_{oc,rad}$ is also calculated by integrating the product of EQE and ϕ_{BB}, and ΔV_{nr} is equal to the difference between $V_{oc,rad}$ and V_{oc}. To avoid an arbitrary fitting on the EQE spectrum, two boundary conditions are applied. Details are provided in ESI-2.† (c) Dependence of J_{sc} of the solar cell on illumination intensity. A slope of one is obtained indicating monomolecular recombination limiting J_{sc} of the solar cell.

PM7:Y5, and we find a linear dependence of J_{sc} on the light intensity, which suggests that the IQE and J_{sc} of the solar cell are limited by inefficient charge carrier generation, a result of monomolecular recombination losses.[47,48]

The monomolecular recombination loss in BHJ solar cells can be associated with inefficient exciton dissociation in the active layer. This is indeed observed for the **PM7:Y5** blend system in the PL quenching measurements. As shown in Fig. 2a, the characteristic PL emission spectra of the neat **PM7** and the neat **Y5** film are peaked at 680 and 920 nm, respectively. In the blend active layer of **PM7:Y5**, the **PM7** emission peak is found completely quenched, but the **Y5** emission peak is only slightly reduced. This suggests that the singlet excitons generated in the **Y5** phase of the blend active layer do not dissociate into free charge carriers. However, the atomic force microscopic image reveals that there is no obvious phase separation in the active layer (ESI-5†), and the efficient quenching of the **PM7** PL emission implies that the degree of phase separation in the active layer is low. Therefore, the reason for the inefficient dissociation of the singlet **Y5** excited state ($S_{1,A}$) is ascribed to the too-small ΔE_{CT} providing an insufficient driving force for the already formed CT state excitons to dissociate, which is very common for the BHJ systems with small ΔE_{CT}.[23–26] In this case, an electric field-dependent PL quenching of the excited state is expected, because dissociation of the weakly bound CT excitons is often facilitated by an electric field, resulting in less populated $S_{1,A}$ states, and thus reduced $S_{1,A}$ emission intensity.[23,24]

The field-dependent PL spectra are measured for the solar cell based on **PM7:Y5**, as well as the photovoltaic device based on pure **Y5** (ESI-6†). In Fig. 2b, the intensities of the emission peak are plotted as a function of applied voltage. We find that for the solar cell based on the blend active layer, the **Y5**

Table 1 Performance parameters of the solar cells based on PM7:Y5, PM7:PBDB-T(10%):Y5, and PBDB-T:Y5. Details regarding the determination of these parameters are provided in ESI-2 (see ESI)

	J_{sc} (mA cm^{-2})	V_{oc} (V)	PCE (%)	$E_{S1,A}$ (eV)	E_{CT} (eV)	ΔE_{CT} (eV)	V_{loss} (V)	$J_{0,rad}$ (mA cm^{-2})	$V_{oc,rad}$ (V)	$\Delta V_{nr}{}^{a}$ (V)	$\Delta V_{nr}{}^{b}$ (V)	EQE_{EL} (%)
PM7:Y5	7.8	0.98	3.28	1.42	1.39	0.03	0.44	1.5×10^{-18}	1.10	0.12	0.13	0.751
PM7:PBDB-T(10%):Y5	12.0	0.95	5.27	1.42	1.39	0.03	0.47	1.3×10^{-18}	1.10	0.15	0.16	0.142
PBDB-T:Y5	17.2	0.88	9.04	1.42	1.37	0.05	0.54	2.7×10^{-18}	1.08	0.21	0.22	0.015

[a] ΔV_{nr} calculated from $J_{0,rad}$. [b] ΔV_{nr} calculated from measured EQE_{EL}.

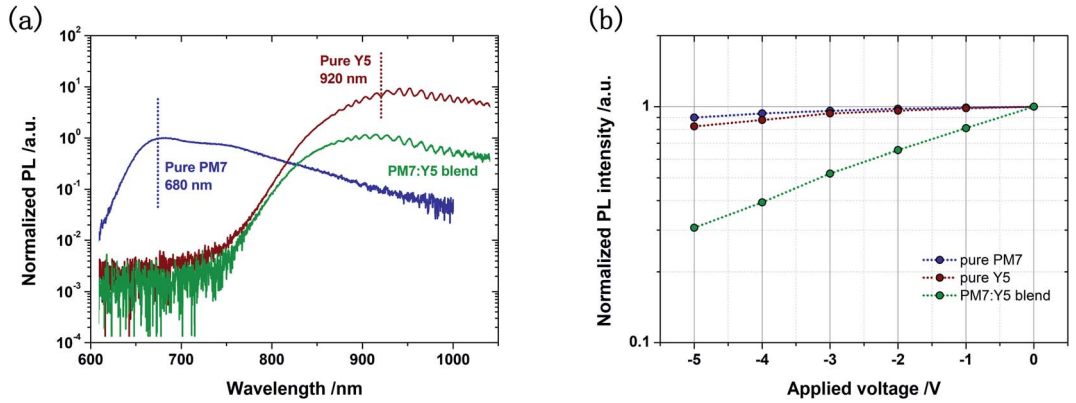

Fig. 2 (a) PL spectra of pure **PM7**, pure **Y5**, and the **PM7**:**Y5** blend, measured with laser excitation at 460 nm. The emission peaks of pure **PM7** and pure **Y5** are located at 680 and 920 nm, respectively, and the PL of the blend is dominated by the **Y5** emission. (b) Emission intensity values of the PL peaks of the solar cells based on pure **PM7**, pure **Y5**, and the **PM7**:**Y5** blend plotted as a function of applied voltage. The intensity values are normalized by the intensity value of the peak measured under short circuit conditions. Complete spectra are provided in ESI-6.†

emission peak at 920 nm is effectively quenched by the applied voltage, whereas the degree of the electric field induced quenching of the emission from the device based on pure **Y5** is significantly smaller. These field-dependent PL results suggest that CT states are indeed formed in the solar cell based on **PM7:Y5**, but they do not easily dissociate into free charge carriers under a short-circuit condition.

The chemical structure of **PBDB-T**[49] is similar to **PM7**, but the highest-occupied-molecular-orbital (HOMO) level of **PBDB-T** (−5.3 eV) is slightly upper laying compared to that of **PM7** (−5.4 eV).[29] Therefore, a higher ΔE_{CT} exists in the solar cell based on the blend of **PBDB-T:Y5**, allowing for more efficient dissociation of CT excitons and higher J_{sc} (Table 1). However, V_{loss} in the solar cell is significantly higher, not only because of the higher ΔE_{CT} but also a higher ΔV_{nr}.

Therefore, to overcome the problem of inefficient CT dissociation in the low V_{loss} solar cell based on **PM7:Y5**, **PBDB-T** is employed as a third component, acting as an additional donor for constructing ternary solar cells. Note that the ternary solar cells based on **PBDB-T:PM7:Y5** are with a fixed donor : acceptor weight ratio (1 : 1.2). The representative *J*–*V* characteristic curves of the solar cells are provided in ESI-7,† and J_{sc} are plotted as a function of the **PBDB-T** content in Fig. 3a. Surprisingly, we find that with the addition of a very small amount of **PBDB-T** (**PBDB-T** : **PM7** donor ratio = 10 wt%), J_{sc} of the solar cell is increased by 30%, from 7 to 10 mA cm^{-2}, which is further doubled, when the donor ratio is increased to 20%. The J_{sc} of the solar cell does not noticeably increase when the donor ratio is increased to over 20%, and when the donor ratio exceeds 40%, J_{sc} is reduced.

These results indicate that the IQE of the ternary solar cell is increased significantly with the **PBDB-T** : **PM7** donor ratio exceeding 20%, which is remarkable as it suggests that adding **PBDB-T** into the **PM7:Y5** blend can lead to substantially more efficient CT state dissociation. Indeed, from Fig. 3b, we find that the PL peak of the blend at 920 nm, corresponding to **Y5** emission, is much more efficiently quenched, and the dependence of the PL intensity on the applied electric field is significantly reduced in the ternary solar cell with **PBDB-T** (Fig. 3c).

There are two possible mechanisms for the increased dissociation efficiency of the CT excitons in the ternary blend:[50] (1) There is no interaction of the frontier orbitals of the different donor materials, and most of the holes generated in **Y5** are transferred to **PBDB-T** to contribute to free charge carrier generation. (2) There is a hybridization of the energy levels of **PBDB-T** and **PM7**, leading to effectively reduced E_{CT} and increased driving force for the whole system. This can result in a decreased electronic coupling strength between $S_{1,A}$ and CT states, and thus reducing the probability for CT states to back transfer to $S_{1,A}$ state, and increasing the dissociation probability of the CT states. Both mechanisms require a homogeneous distribution of **PBDB-T** in the blend active layer.

When there is no interaction between the orbitals of the donor materials in the ternary solar cells, the recombination dynamics of the photogenerated charge carriers should be primarily determined by the electronic property of the CT state formed at the **PBDB-T:Y5** interfaces, even when the blend is with a low **PBDB-T** content since the **PBDB-T:Y5** CT state is the lowest energy of state in the blend system. Therefore, with a small amount of **PBDB-T** in the ternary blend, V_{oc} of the solar cell should be similar to that of the binary solar cell based on **PBDB-T:Y5**. In addition, the characteristics of the recombination current of the ternary solar cell should be the same as that of the binary solar cell based on **PBDB-T:Y5**. Because in the ternary solar cell, the electrically injected holes are expected to rapidly relax to the HOMO of **PBDB-T**, and then find electrons at the **PBDB-T:Y5** interfaces to recombine. However, we observe that V_{oc} of the ternary solar cell almost linearly decreases with the increasing **PBDB-T** content (Fig. 3a), and the recombination current in the solar cell gradually increases with the **PBDB-T** content (ESI-7†). These results indicate that the energy levels of **PBDB-T** and **PM7** are hybridized to form an effective CT state in the ternary blend, which are also observed for other ternary blends reported in literature.[50]

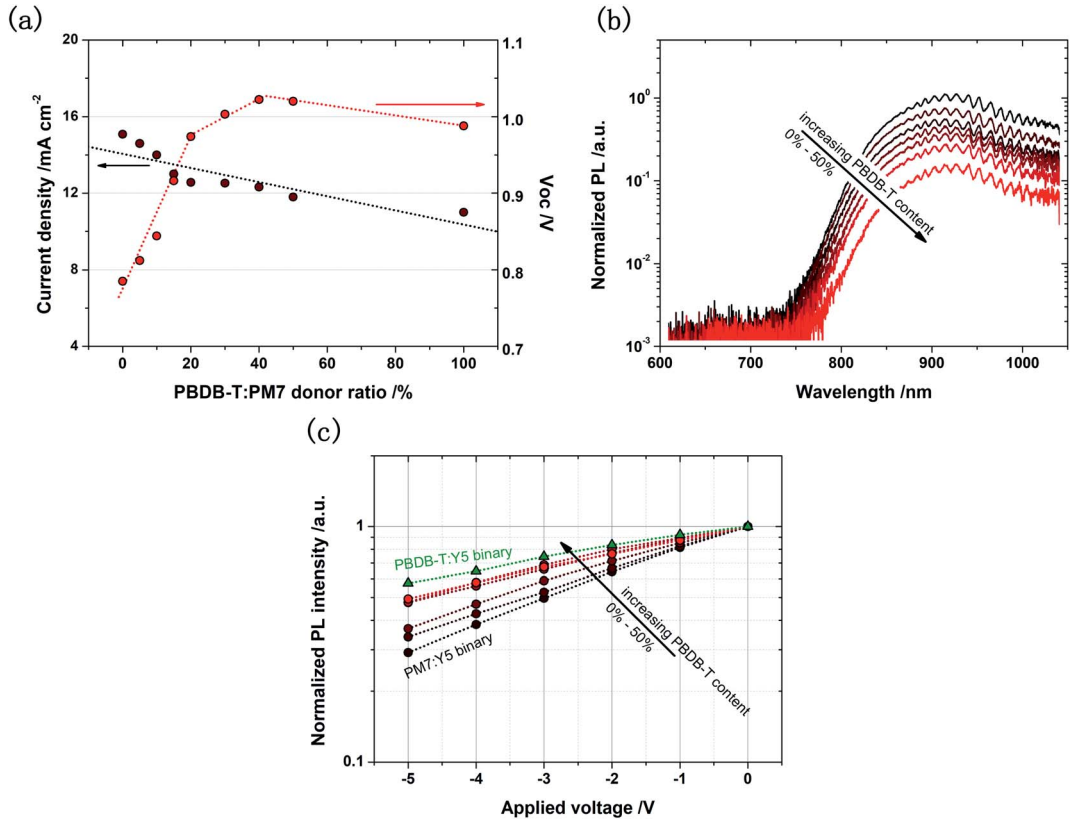

Fig. 3 (a) J_{sc} and V_{oc} of the solar cells based on PBDB-T:PM7:Y5, plotted as a function of the PBDB-T : PM7 donor ratio. (b) PL emission spectra of the solar cell based on different PBDB-T : PM7 donor ratios. More efficient quenching of the Y5 emission is found in the solar cell with higher PBDB-T content. (c) Emission intensities of the PL peaks of the solar cells based on different PBDB-T : PM7 donor ratios plotted as a function of applied voltage. The intensity values are normalized by the intensity value of the peak measured under short circuit conditions. The dependence of the PL quenching efficiency on the applied voltage reduces with the increasing PBDB-T content. Complete spectra are provided in ESI-6.†

To elucidate that the energy levels of the **PBDB-T** and **PM7** in the blend are hybridized, we further investigate the charge generation process in the devices based on **PBDB-T : PM7**. We find that the J_{sc} and EQE of the device based on **PBDB-T : PM7** (1 : 1 wt%) are considerably higher than that of the device based on pure **PBDB-T** or pure **PM7** (Fig. S11a and b, ESI†), but the absorption spectra of the two materials are very similar (Fig. S3b†). PL measurements, shown in Fig. S11c (ESI),† suggest that the emissions from **PBDB-T** and **PM7** are significantly quenched, in the blend of **PBDB-T:PM7**. This suggests that the singlet excited states of **PBDB-T** and **PM7** are hybridized, resulting in the formation of CT states at the interface between the two polymers, facilitating the dissociation of the excitons generated in the blend active layer. Sensitive electroluminescence and EQE measurements (Fig. S11d and e, ESI†) reveal that the absorption and emission spectra of the blend thin film are slightly red-shifted compared to those of the films based on pure **PBDB-T** or **PM7**, also confirming that the energy of the excited states, *i.e.*, the energy levels of **PBDB-T** and **PM7** are hybridized in the blend.

Therefore, we can also use the Marcus theory to evaluate the CT state property in the ternary solar cells (SI-2). We find that E_{CT} is indeed gradually reduced with the increasing **PBDB-T** content (Fig. 4a), leading to a continuously tuned ΔE_{CT} (Fig. 4b). The electronic coupling between the $S_{1,A}$ and CT state is thus reduced.

Inevitably, the V_{oc} of the ternary solar cell reduces with increasing **PBDB-T** content (Fig. 4c). However, due to the hybridization of the energy levels of **PBDB-T** and **PM7**, the V_{oc} does not directly reduce to that of the binary solar cell based on **PBDB-T:Y5**. Therefore, the low V_{loss} property of the solar cell based on **PM7:Y5** can be well kept in the ternary solar cell, while QE of the solar cell is significantly increased, with the addition of a small amount of **PBDB-T**. As shown in Fig. 4c, V_{loss} is about 0.47 V in the ternary solar cell with a **PBDB-T : PM7** donor ratio of 10%, which is slightly higher than that of the binary solar cell based on **PM7:Y5** (0.44 eV), but the J_{sc} of the ternary solar cell is higher by a factor of 1.30; and the V_{loss} is increased to 0.50 V for the ternary solar cell with a donor ratio of 20%, while the J_{sc} is doubled. The gain of using the ternary blend strategy is remarkably high.

The increased V_{loss} in the ternary solar cell is partially due to the reduced effective E_{CT}, since E_{CT} is the electronic bandgap of the blend active layer.[12] Meanwhile, the reduced E_{CT} can lead to increased ΔV_{nr} due to a stronger vibrational coupling between the excited and ground state.[17] In addition, the electronic coupling between the $S_{1,A}$ and CT state is reduced due to the reduced E_{CT}: although the reduction in the electronic coupling

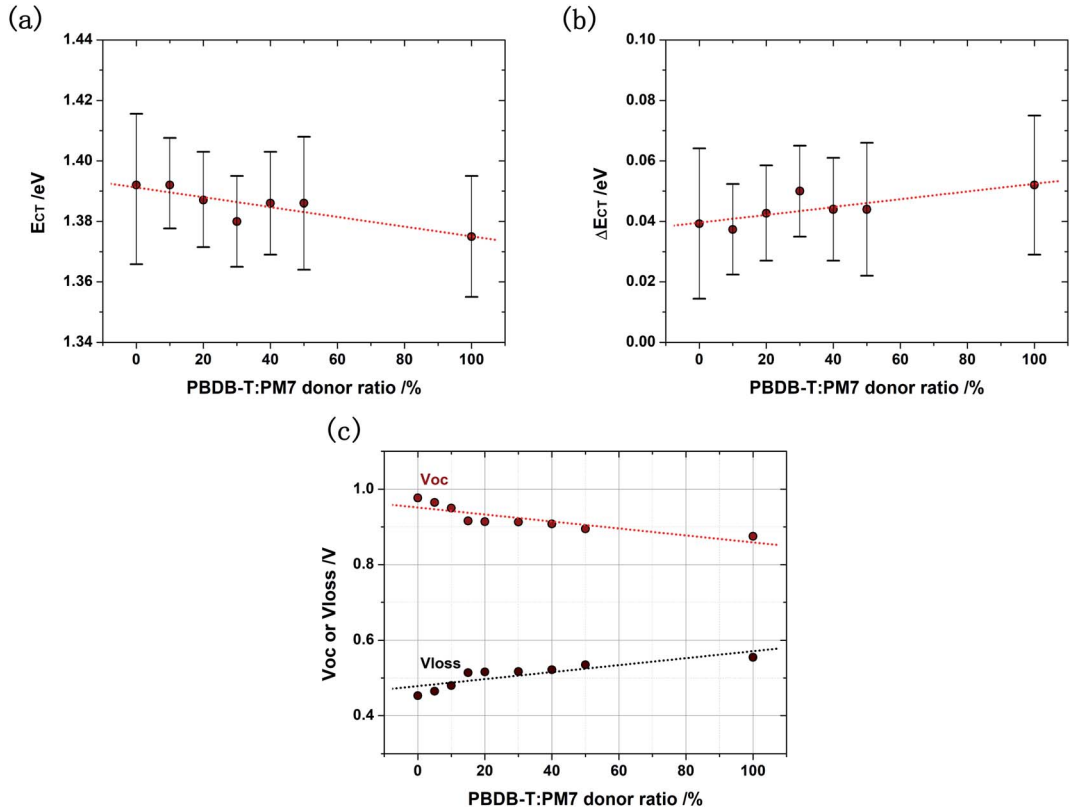

Fig. 4 (a) E_{CT} and (b) ΔE_{CT} of the solar cells based on **PBDB-T**:**PM7**:**Y5**, plotted as a function of the **PBDB-T** : **PM7** donor ratio. (c) V_{oc} and V_{loss} of the solar cells based on **PBDB-T**:**PM7**:**Y5**, plotted as a function of the **PBDB-T** : **PM7** donor ratio. Note that the donor : acceptor ratio for the ternary blends is also kept at 1 : 1.2 (weight ratio).

is needed to prevent the back transfer of the CT state to the $S_{1,A}$ state, the reduced coupling can also lead to a reduced the effective dipole moment for the CT to ground state transition,[19] resulting in the increased non-radiative decay rate of CT state, reduced EQE_{EL}, and thus increased ΔV_{nr} in the solar cell. EQE_{EL} measurements (Fig. S8, ESI†) confirm that ΔV_{nr} in the ternary solar cell is indeed higher than that in the binary solar cell based on **PM7**:**Y5**, and it gradually increases with the **PBDB-T** content, as shown in Fig. 5a, and transient photovoltage decay time plotted as a function of bias illumination intensity

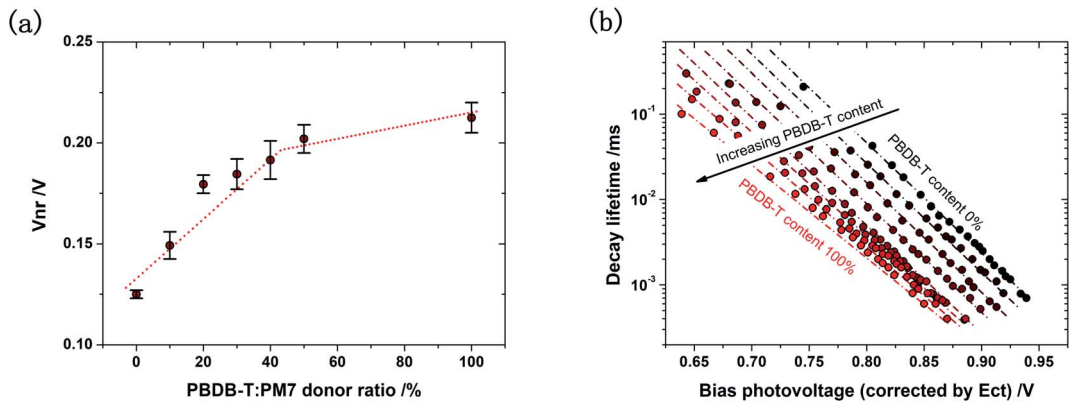

Fig. 5 (a) ΔV_{nr} of the solar cells based on **PBDB-T**:**PM7**:**Y5** with different **PBDB-T** : **PM7** donor ratios. The ΔV_{nr} values are calculated from the measured V_{oc} and $V_{oc,rad}$ determined from the sensitive EQE spectra, and they are verified by EQE_{EL} measurements. (b) Transient photovoltage decay lifetime measured with a pulsed LED and a bias illumination at different intensities for the solar cells with different **PBDB-T** : **PM7** donor ratios. The *x*-axis represents the photovoltage of the solar cell generated by the bias illumination. To compare the decay lifetime at the same charge carrier concentration, the *x*-axis is corrected for the difference in E_{CT} of the solar cells based on different **PBDB-T** contents. Photovoltage *vs.* time plots for these solar cells are provided in ESI-9.†

confirms that the increased ΔV_{nr} is a result of the increased non-radiative decay rate of CT state (Fig. 5b).

3. Conclusion

To conclude, we investigated organic solar cells based on **PM7**:**Y5**, in which an extremely low V_{loss} (0.44 V) was found, and we showed that the low V_{loss} was a result of a small ΔE_{CT} and a low ΔV_{nr}. However, the QE of the solar cell was low, due to the small ΔE_{CT}, leading to inefficient dissociation of CT state excitons. To solve this problem, a ternary blend strategy was employed. We demonstrated that the use of **PBDB-T** with slightly upper laying HOMO, compared to **PM7**, as a second donor in the blend active layer could effectively lead to a hybridization of the energy levels of **PBDB-T** and **PM7**. This resulted in reduced E_{CT} and increased ΔE_{CT} in the ternary system, giving rise to a significantly improved CT state dissociation efficiency in the active layer, and thus an increased J_{sc} of the solar cell. More importantly, the low V_{loss} property of the **PM7**:**Y5** based blend was very well maintained: J_{sc} of the ternary solar cell with a **PBDB-T** : **PM7** donor ratio of 20% was increased by two folds, compared to that of the binary solar cell based on **PM7**, but V_{loss} was only increased by 0.06 eV. Thus, we propose that the ternary blend strategy is highly effective for realizing a balance between QE and V_{loss} in organic solar cells with a small ΔE_{CT}. To achieve a high degree of hybridization of the energy levels of the active materials, and the tuning of ΔE_{CT} of the ternary blend, the second donor should have different energy levels compared to the primary donor, and the chemical structures of the donor materials should be similar to allow a high degree of intermixing in the ternary blend. This is a newly discovered advantage of the ternary blend strategy, which has not yet been fully explored.

4. Experimental

Materials and devices

PEDOT:PSS (CLEVIOS P VP AL 4083) was purchased from Heraeus, **PBDB-T**, **PM7**, **Y5** and PFN-Br were purchased from Solarmer. The solar cells are based on a standard architecture of ITO/PEDOT:PSS active layer/PFN-Br/Ag. The indium tin oxide (ITO) substrates were sonicated with acetone, isopropanol, and ethanol, and then rinsed with deionized water. PEDOT:PSS interlayers were spin-coated on the clean ITO substrates at a spin-coating speed of 5000 rpm for 60 s, and annealed on a hotplate at 150 °C for 20 min. The thickness of the PEDOT:PSS interlayers was about 30 nm. The organic photoactive layers (100 nm) were spin-coated onto the PEDOT:PSS coated substrate in a glovebox filled with nitrogen, at a speed of 2000 rpm for 30 s, from chloroform solutions with a total concentration of the active materials of 8 mg mL^{-1} (the donor : acceptor weight ratio is kept to 1 : 1.2 for both the binary and the ternary systems). The solutions were stirred at 40 °C for 4 hours, prior to use, and the active layers were annealed at 110 °C for 10 min in the glove box. Then, the PFN–Br interlayers (1 nm) were spin-coated on the active layers at a spin-coating speed of 3000 rpm for 30 s. Construction of the solar cells was finalized by a thermal evaporation of 100 nm Ag electrode in a vacuum chamber at a pressure of 1×10^{-6} Pa. The photoactive area of the solar cells is about 4 mm^2.

Characterizations

Details regarding characterization of the materials and devices are provided in ESI (ESI-1).†

Conflicts of interest

The authors declare no competing financial interest.

Acknowledgements

This work is financial supported by the National Natural Science Foundation of China (Grant No. 51973031, 51933001, 52073056), Shanghai Pujiang Program (Grant No. 19PJ1400500), the Natural Science Foundation of Shanghai (Grant No. 19ZR1401400) and the Fundamental Research Funds for the Central Universities (Grant No. 2232021A09).

References

1 Q. Liu, Y. Jiang, K. Jin, J. Qin, J. Xu, W. Li, J. Xiong, J. Liu, Z. Xiao, K. Sun, S. Yang, X. Zhang and L. Ding, *Sci. Bull.*, 2020, **65**, 272–275.
2 H. N. Tran, S. Park, F. T. A. Wibowo, N. V. Krishna, J. H. Kang, J. H. Seo, H. Nguyen-Phu, S. Jang and S. Cho, *Adv. Sci.*, 2020, **7**, 2002395.
3 L. Meng, Y. Zhang, X. Wan, C. Li, X. Zhang, Y. Wang, X. Ke, Z. Xiao, L. Ding, R. Xia, H.-L. Yip, Y. Cao and Y. Chen, *Science*, 2018, **361**, 1094–1098.
4 Y. Cui, H. Yao, J. Zhang, K. Xian, T. Zhang, L. Hong, Y. Wang, Y. Xu, K. Ma, C. An, C. He, Z. Wei, F. Gao and J. Hou, *Adv. Mater.*, 2020, **32**, 1908205.
5 Q. An, F. Zhang, J. Zhang, W. Tang, Z. Deng and B. Hu, *Energy Environ. Sci.*, 2016, **9**, 281–322.
6 N. Gasparini, A. Salleo, I. McCulloch and D. Baran, *Nat. Rev. Mater.*, 2019, **4**, 229–242.
7 P. Bi and X. Hao, *Sol. RRL*, 2019, **3**, 1800263.
8 P. Chao, H. Chen, Y. Zhu, H. Lai, D. Mo, N. Zheng, X. Chang, H. Meng and F. He, *Adv. Mater.*, 2020, **32**, 1907059.
9 W. Gao, H. Fu, Y. Li, F. Lin, R. Sun, Z. Wu, X. Wu, C. Zhong, J. Min, J. Luo, H. Y. Woo, Z. Zhu and A. K. -Y. Jen, *Adv. Energy Mater.*, 2020, 2003177.
10 J. Yuan, Y. Zhang, L. Zhou, G. Zhang, H.-L. Yip, T.-K. Lau, X. Lu, C. Zhu, H. Peng, P. A. Johnson, M. Leclerc, Y. Cao, J. Ulanski, Y. Li and Y. Zou, *Joule*, 2019, **3**, 1140–1151.
11 K. Vandewal, K. Tvingstedt, A. Gadisa, O. Inganäs and J. V. Manca, *Nat. Mater.*, 2009, **8**, 904–909.
12 K. Vandewal, K. Tvingstedt, A. Gadisa, O. Inganäs and J. V. Manca, *Phys. Rev. B: Condens. Matter Mater. Phys.*, 2010, **81**, 125204.
13 Z. Tang, J. Wang, A. Melianas, Y. Wu, R. Kroon, W. Li, W. Ma, M. R. Andersson, Z. Ma, W. Cai, W. Tress and O. Inganäs, *J. Mater. Chem. A*, 2018, **6**, 12574–12581.

14 K. Vandewal, K. Tvingstedt and O. Inganäs, in *Semiconductors and Semimetals*, Elsevier, 2011, vol. 85, pp. 261–295.
15 M. Azzouzi, J. Yan, T. Kirchartz, K. Liu, J. Wang, H. Wu and J. Nelson, *Phys. Rev. X*, 2018, **8**, 031055.
16 D. Qian, Z. Zheng, H. Yao, W. Tress, T. R. Hopper, S. Chen, S. Li, J. Liu, S. Chen, J. Zhang, X.-K. Liu, B. Gao, L. Ouyang, Y. Jin, G. Pozina, I. A. Buyanova, W. M. Chen, O. Inganäs, V. Coropceanu, J.-L. Bredas, H. Yan, J. Hou, F. Zhang, A. A. Bakulin and F. Gao, *Nat. Mater.*, 2018, **17**, 703–709.
17 J. Benduhn, K. Tvingstedt, F. Piersimoni, S. Ullbrich, Y. Fan, M. Tropiano, K. A. McGarry, O. Zeika, M. K. Riede, C. J. Douglas, S. Barlow, S. R. Marder, D. Neher, D. Spoltore and K. Vandewal, *Nat. Energy*, 2017, **2**, 17053.
18 K. D. Rosenthal, M. P. Hughes, B. R. Luginbuhl, N. A. Ran, A. Karki, S.-J. Ko, H. Hu, M. Wang, H. Ade and T.-Q. Nguyen, *Adv. Energy Mater.*, 2019, **9**, 1901077.
19 F. D. Eisner, M. Azzouzi, Z. Fei, X. Hou, T. D. Anthopoulos, T. J. S. Dennis, M. Heeney and J. Nelson, *J. Am. Chem. Soc.*, 2019, **141**, 6362–6374.
20 K. Vandewal, *Annu. Rev. Phys. Chem.*, 2016, **67**, 113–133.
21 V. Coropceanu, X.-K. Chen, T. Wang, Z. Zheng and J.-L. Brédas, *Nat. Rev. Mater.*, 2019, **4**, 689–707.
22 K. Vandewal, K. Tvingstedt, J. V. Manca and O. Inganäs, *IEEE J. Sel. Top. Quantum Electron.*, 2010, **16**, 1676–1684.
23 K. Vandewal, Z. Ma, J. Bergqvist, Z. Tang, E. Wang, P. Henriksson, K. Tvingstedt, M. R. Andersson, F. Zhang and O. Inganäs, *Adv. Funct. Mater.*, 2012, **22**, 3480–3490.
24 Z. Ma, W. Sun, S. Himmelberger, K. Vandewal, Z. Tang, J. Bergqvist, A. Salleo, J. W. Andreasen, O. Inganäs, M. R. Andersson, C. Müller, F. Zhang and E. Wang, *Energy Environ. Sci.*, 2013, **7**, 361–369.
25 C. Yang, J. Zhang, N. Liang, H. Yao, Z. Wei, C. He, X. Yuan and J. Hou, *J. Mater. Chem. A*, 2019, **7**, 18889–18897.
26 Y. Xie and H. Wu, *Materials Today Advances*, 2020, **5**, 100048.
27 L. Benatto, M. de J. Bassi, L. C. W. de Menezes, L. S. Roman and M. Koehler, *J. Mater. Chem. C*, 2020, **8**, 8755–8769.
28 S. Ullbrich, J. Benduhn, X. Jia, V. C. Nikolis, K. Tvingstedt, F. Piersimoni, S. Roland, Y. Liu, J. Wu, A. Fischer, D. Neher, S. Reineke, D. Spoltore and K. Vandewal, *Nat. Mater.*, 2019, **18**, 459–464.
29 H. Zhang, H. Yao, J. Hou, J. Zhu, J. Zhang, W. Li, R. Yu, B. Gao, S. Zhang and J. Hou, *Adv. Mater.*, 2018, **30**, 1800613.
30 J. Yuan, Y. Zhang, L. Zhou, C. Zhang, T.-K. Lau, G. Zhang, X. Lu, H.-L. Yip, S. K. So, S. Beaupré, M. Mainville, P. A. Johnson, M. Leclerc, H. Chen, H. Peng, Y. Li and Y. Zou, *Adv. Mater.*, 2019, **31**, 1807577.
31 M.-A. Pan, T.-K. Lau, Y. Tang, Y.-C. Wu, T. Liu, K. Li, M.-C. Chen, X. Lu, W. Ma and C. Zhan, *J. Mater. Chem. A*, 2019, **7**, 20713–20722.
32 R. Ma, T. Liu, Z. Luo, Q. Guo, Y. Xiao, Y. Chen, X. Li, S. Luo, X. Lu, M. Zhang, Y. Li and H. Yan, *Sci. China: Chem.*, 2020, **63**, 325–330.
33 R. A. Marcus, *J. Phys. Chem.*, 1989, **93**, 3078–3086.
34 I. R. Gould, D. Noukakis, L. Gomez-Jahn, R. H. Young, J. L. Goodman and S. Farid, *Chem. Phys.*, 1993, **176**, 439–456.
35 W. Shockley and H. J. Queisser, *J. Appl. Phys.*, 1961, **32**, 510–519.
36 Z. Tang, Z. Ma, A. Sánchez-Díaz, S. Ullbrich, Y. Liu, B. Siegmund, A. Mischok, K. Leo, M. Campoy-Quiles, W. Li and K. Vandewal, *Adv. Mater.*, 2017, **29**, 1702184.
37 K. Vandewal, J. Benduhn and V. C. Nikolis, *Sustainable Energy Fuels*, 2018, **2**, 538–544.
38 U. Rau, *Phys. Rev. B: Condens. Matter Mater. Phys.*, 2007, **76**, 085303.
39 Y. Xu, H. Yao, L. Ma, J. Wang and J. Hou, *Rep. Prog. Phys.*, 2020, **83**, 082601.
40 J. Wang, H. Yao, Y. Xu, L. Ma and J. Hou, *Mater. Chem. Front.*, 2021, **5**, 709–722.
41 L. A. A. Pettersson, L. S. Roman and O. Inganäs, *J. Appl. Phys.*, 1999, **86**, 487–496.
42 G. F. Burkhard, E. T. Hoke, S. R. Scully and M. D. McGehee, *Nano Lett.*, 2009, **9**, 4037–4041.
43 J. Vollbrecht, V. V. Brus, S.-J. Ko, J. Lee, A. Karki, D. X. Cao, K. Cho, G. C. Bazan and T.-Q. Nguyen, *Adv. Energy Mater.*, 2019, **9**, 1901438.
44 G.-J. A. H. Wetzelaer, N. J. V. der Kaap, L. J. A. Koster and P. W. M. Blom, *Adv. Energy Mater.*, 2013, **3**, 1130–1134.
45 L. J. A. Koster, V. D. Mihailetchi and P. W. M. Blom, *Appl. Phys. Lett.*, 2006, **88**, 052104.
46 G. Lakhwani, A. Rao and R. H. Friend, *Annu. Rev. Phys. Chem.*, 2014, **65**, 557–581.
47 P. Hartnagel and T. Kirchartz, *Adv. Theory Simul.*, 2020, **3**, 2000116.
48 A. K. K. Kyaw, D. H. Wang, V. Gupta, W. L. Leong, L. Ke, G. C. Bazan and A. J. Heeger, *ACS Nano*, 2013, **7**, 4569–4577.
49 D. Qian, L. Ye, M. Zhang, Y. Liang, L. Li, Y. Huang, X. Guo, S. Zhang, Z. Tan and J. Hou, *Macromolecules*, 2012, **45**, 9611–9617.
50 W. Tress, B. Beyer, N. Ashari Astani, F. Gao, S. Meloni and U. Rothlisberger, *J. Phys. Chem. Lett.*, 2016, **7**, 3936–3944.